

Monte Carlo simulated dynamical magnetization of single-chain magnets

Jun Li and Bang-Gui Liu*

*Beijing National Laboratory for Condensed Matter Physics,
Institute of Physics, Chinese Academy of Sciences, Beijing 100190, China*

(Dated: February 13, 2020)

Here, a dynamical Monte-Carlo (DMC) method is used to study temperature-dependent dynamical magnetization of famous Mn_2Ni system as typical example of single-chain magnets with strong magnetic anisotropy. Simulated magnetization curves are in good agreement with experimental results under typical temperatures and sweeping rates, and simulated coercive fields as functions of temperature are also consistent with experimental curves. Further analysis indicates that the magnetization reversal is determined by both thermal-activated effects and quantum spin tunnelings. These can help explore basic properties and applications of such important magnetic systems.

PACS numbers: 75.75.-c, 05.10.-a, 75.78.-n, 75.10.-b, 75.90.+w

Various nanoscale spin chains have been attracting great attention because of their important properties and potential applications in information science and technology[1–5]. The single-chain magnet (SCM) is a new member of such nanoscale spin chains, and its basic spin unit come from some transition-metal or rare-earth ions combined with appropriate organic molecules[2–14]. A famous SCM is the $[\text{Mn}_2\text{Ni}]$ system[3–7], with $\text{C}_{62}\text{H}_{64}\text{N}_{10}\text{O}_{14}\text{Cl}_2\text{Mn}_2\text{Ni}$ and $\text{C}_{60}\text{H}_{66}\text{N}_{12}\text{O}_{14}\text{Cl}_2\text{Mn}_2\text{Ni}$ as two typical formula units with spin $S = 3$. A well-known Arrhenius law has been observed for their spin relaxation at high enough temperature [15, 16]. On the other hand, at low enough temperature, quantum Landau-Zener (LZ) spin tunneling should play important roles in their spin reversal[17, 18]. Such phenomena can be investigated by using some methods for single-molecule magnets[19–28]. As for SCM systems, inter-spin exchange interactions play important roles and thermal effects can cause Glauber spin dynamics[5, 6], which was originally proposed for one-dimensional Ising spin model[29–31]. Furthermore, a systematical experimental study shows that quantum nucleation can become important to reverse single spins, create domains of reversed spins, and reverse the whole SCM[7]. Therefore, it is useful to elucidate what roles these play in determining dynamical magnetization of SCM systems.

Here, we use the hybrid DMC method and thereby investigate the $[\text{Mn}_2\text{Ni}]$ SCM system as a typical example of SCMs, taking both classical and quantum effects into account. Our results for typical temperatures and sweeping rates are consistent with corresponding experimental curves. It is very interesting that we can satisfactorily fit the simulated and experimental B_c - T curves by one simple function. These means that the DMC method and simulated results are both reasonable and reliable for such SCM systems. Furthermore, we explain magnetization reversal modes for different temperatures on the basis of our simulated results and analyses. More detailed results will be presented in the following.

The single-chain magnet can be considered a one-

dimensional composite spin lattice whose spins can be constructed by repeating a basic unit of $[\text{Mn}_2\text{Ni}]$: Mn-Ni-Mn (or $\text{Mn}^{3+}\text{-Ni}^{2+}\text{-Mn}^{3+}$). The antiferromagnetic Ni-Mn interaction is much stronger than the ferromagnetic Mn-Mn one so that the low-temperatures physics of this spin chain can be modelled by an effective ferromagnetic chain of the units of $[\text{Mn}_2\text{Ni}]$ ($S = 3$) with spin interaction only between the nearest units[3, 4, 6–12].

The ferromagnetic spin Hamiltonian can be expressed as[7, 9, 14]

$$\hat{H} = \hat{H}_0 - \sum_{i=1}^{N-1} J \hat{S}_i \cdot \hat{S}_{i+1} - \sum_{i=1}^N g \mu_B B_z \hat{S}_i^z \quad (1)$$

where g is the Lande g factor ($g = 2$ is used), μ_B the Bohr magneton, J (> 0) the ferromagnetic exchange constant. $\hat{S}_i = \{\hat{S}_i^x, \hat{S}_i^y, \hat{S}_i^z\}$ is the spin vector operator for the i -th Mn_2Ni unit, and

$$\hat{H}_0 = \sum_{i=1}^N \{-D(\hat{S}_i^z)^2 - E[(\hat{S}_i^x)^2 - (\hat{S}_i^y)^2]\} \quad (2)$$

is the Hamiltonian for the isolated ferromagnetic spin.

D and E are the anisotropic parameters. As for the parameters of the spin interaction and on-site anisotropy, we use $J/k_B=1.56\text{K}$ and $D/k_B=2.5\text{K}$ from thermodynamical measurements[7, 9, 14]. The transverse anisotropic parameter E is much smaller, but necessary to realize the Landau-Zener spin tunnelling. We take $E/k_B=0.1\text{K}$ by comparing our simulated results with experimental ones.

We use a dynamical Monte Carlo method to simulate the spin dynamics of the interacting spin system under sweeping magnetic field[28, 32, 33]. At the beginning, we set all of the spins at the state $S^z = -3$.

We divide the time t into small time steps with a step length Δt and describe the Monte Carlo time points with $t(n)$, where n takes 0, 1, 2, 3,.... The magnetic field starts from $-B_0$ and increases by an increment of $\Delta t \cdot \nu$ until B_0 . The spin can be reversed within a Monte Carlo step (MCS) through the two reversal mechanisms.

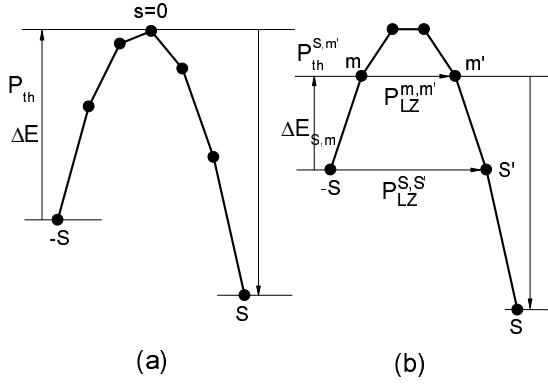


FIG. 1: A schematic of the three spin reversal mechanisms: Thermal-activated barrier hurdling (a), direct and thermal-assisted LZ tunnelings (b). The horizontal solid line with arrow means that the two energy levels satisfy the resonance conditions. The probabilities, energy levels, barrier, and other symbols are defined in the text.

For the classical thermal activation, we can obtain the following probability P_{th} that within the time decrement Δt [15, 16].

$$P_{th} = 1 - \exp(-R_i \Delta t) \quad (3)$$

Where $R_i = R_0 \exp(\frac{-\Delta E_i}{k_B T})$ is the transition rate, k_B is the Boltzmann constant, T temperature, and R_0 the characteristic frequency for the spin system ($3 \times 10^8 \text{s}^{-1}$). ΔE_i is the potential barrier of the i -th spin between $S_i^z = -3$ and $S_i^z = 3$, as shown in Fig. 1.

There is a necessary condition for a LZ tunnelling of a spin to occur: one of the spin energy levels on the side must be equivalent to another, for example, $E_m(t) = E_{m'}(t)$, as shown in Fig. 1. With the neighboring spins taken into account, such conditions are satisfied at the given magnetic fields[28]. The corresponding LZ transition probability is given by

$$P_{LZ}^{m,m'} = 1 - \exp\left[-\frac{\pi(\Delta_{m,m'})^2}{2\hbar g \mu_B |m - m'| \nu}\right] \quad (4)$$

where the tunnelling splitting $\Delta_{mm'}$ is the energy gap at the avoided crossing of states m and m' , and ν denotes the sweeping rate of the magnetic field.

When m equals to $S = -3$ and m' is S' , we obtain a direct LZ tunnelling with the probability $P_{LZ}^d = P_{LZ}^{S,S'}$. For other possible LZ tunnelling to happen, the spin at first must be excited from $S^z = -3$ to the m values through some thermal activations, as shown in Fig. 1. Considering the thermal probability $P_{th}^{S,m}$ which can be obtained by using the expressions (3), the probability of spin reversal in this channel, P_{LZ}^m , is given by $P_{LZ}^m = P_{th}^{S,m} \cdot P_{LZ}^{m,m'}$. All the three spin-reversal channels are combined to give the total probability for a spin reversal[28]:

$$P^{tot} = 1 - (1 - P_{th}) \cdot (1 - P_{LZ}^d) \cdot \prod_m (1 - P_{LZ}^m) \quad (5)$$

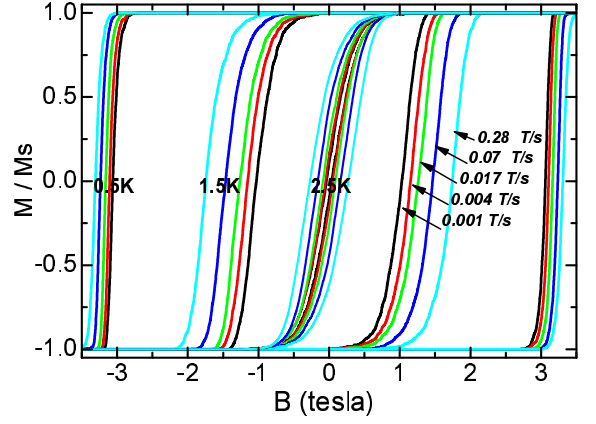


FIG. 2: Hysteresis loops (normalized magnetization (M/M_s) curves against the sweeping field B) for three temperatures: 0.5, 1.5, and 2.5 K. For every temperature, five magnetization curves are plotted with five field sweeping rates: 0.001, 0.004, 0.017, 0.07, and 0.28 tesla/s (from the innermost loop to the outermost for each temperature).

In our simulations, we take $\Delta t = 0.1 \text{ms}$ and use 100 units of Mn_2Ni with free boundary condition. The magnetization is calculated by averaging S_i^z over the 100 spin sites. Each data point is calculated by averaging 10000 independent runs to reduce possible errors. The value of B_0 is made large enough to obtain complete hysteresis loops with the help of a symmetrization treatment.

Presented in Fig. 2 are our typical simulated magnetization curves for five different field sweeping rates ν (0.001, 0.004, 0.017, 0.07, and 0.28 tesla/s) at three different temperatures T : 2.5, 1.5, and 0.5 K. The simulated results show that the hysteresis loops are strongly dependent on both temperature T and field sweeping rate ν . Our simulation shows that there is no hysteresis loop for all the field sweeping rates when temperature reaches 3 K, and at 2.5 K, the thermal effects are dominant and spins can be easily reversed, which results in very small hysteresis loops. Our data analysis indicates that when the temperature further decreases, the thermal-activated spin reversal becomes less important and the thermal-assisted LZ spin tunnelling already takes place frequently. At 1.5 K, another typical temperature, these two channels are available for the spin being reversed, but the total reversal probability is less than that of 2.5 K, and hence the coercive fields is substantially larger than that of 2.5 K. When the temperature becomes very low, for example down to 0.5 K, our probability analysis reveals that the thermal activation is almost frozen and the spin reversal can be realized only through the direct LZ spin tunnelling, and as a result, the coercive fields are large because the transverse parameter E is very small. Even at this low temperature, there is no clear step structure in the magnetization curves, which should be attributed to the strong spin exchange interaction in the J -term.

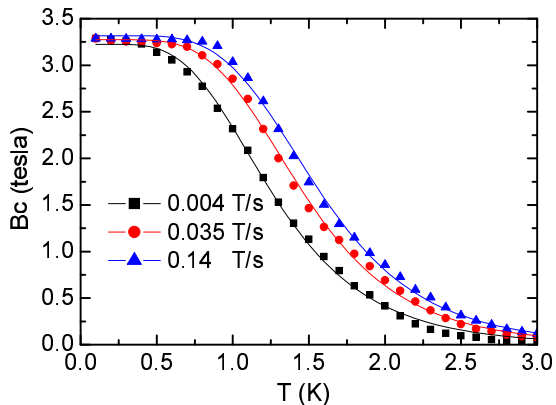


FIG. 3: Temperature (T) dependence of the coercive fields (B_c) for the three field sweeping rates: 0.004, 0.035, and 0.14 tesla/s. The curves are well fitted with Eq. (6) using the set of parameters (A, T_1, T_2) presented in Table I.

This is in contrast to those in the cases of Mn_{12} and Fe_8 systems[19, 20, 28]. Our simulated magnetization curves also show that the larger the field sweeping rate, the larger the hysteresis loop. This trend can be explained by considering that larger sweeping rate means shorter time for spins to try towards reversal, as shown in classical nanoscale spin systems[32, 33].

Furthermore, we have done more simulations with more field sweeping rates and more temperatures. In Fig. 3 we present our systematical results on the coercive fields B_c as functions of temperature T for three sweeping rates ν : 0.004, 0.035, and 0.14 tesla/s. For all the three field sweeping rates, it is clear that the coercive fields decrease with temperature increasing. It is very interesting that these B_c - T curves can be well fitted by the following simple function.

$$B_c = \frac{A}{1 + \exp\left(\frac{T}{T_1} - \frac{T_2}{T}\right)} \quad (6)$$

For the three B_c - T curves in Fig. 3, the fitting parameters (A, T_1, T_2) are summarized in Table I. When the temperature is high, the B_c - T curves are dominated by the T_1 term in the exponential, $B_c \sim A \exp(-\frac{T}{T_1})$, which should be naturally attributed to thermal activations. When the temperature is below 1 K, the coercive fields substantially deviate from classical behavior. Especially when the temperature decreases below 0.5 K, the coercive fields tend to saturate, $B_c \sim A$. This means that the low-temperature saturation behavior is consistent with quantum LZ effect, in contrast with Glauber dynamics[29–31].

It is very surprising that the simple function (6) can satisfactorily describe the experimental B_c - T curves for such sweeping rates, too. Our fitted parameters for the experimental curves are summarized in Table II.

In high-temperature region, the magnetization rever-

TABLE I: Fitting parameters of the three theoretical B_c - T curves in Fig. 3 in terms of the function defined in Eq. (6).

ν (tesla/s)	A (tesla)	T_1 (K)	T_2 (K)
0.004	3.22	0.62	2.54
0.035	3.27	0.65	3.27
0.14	3.31	0.67	3.63

sal is characterized by easy classical end-site nucleation and fast classical wall-moving growth of the reversed spin domain. At intermediate temperature such as 1.5 K, the magnetization reversal is realized by many-site quantum nucleations and classical wall-moving growth of the reversed spin domains. In the low-temperature region, the magnetization reversal is due to frequent many-site quantum nucleations of the reversed-spin domains and these domains are effectively merged by subsequent spin tunnelings. Importantly, it can lead to crossover between these three modes to change temperature. Therefore, the three modes have already been unified into one mechanism in terms of our theory (our model treatment plus our simulation).

TABLE II: Fitting parameters of the three experimental[7, 9, 14] B_c - T curves in terms of the function defined in Eq. (6).

ν (tesla/s)	A (tesla)	T_1 (K)	T_2 (K)
0.004	2.63	0.63	2.85
0.035	2.82	0.70	2.99
0.14	2.97	0.75	3.08

As are clearly shown in Table II, our theoretical parameters are in good agreement with those from experimental data[7, 9, 14]. In addition, we consider a three-dimensional spin system by introducing a very weak inter-chain spin exchange coupling. Our Monte Carlo simulation indicates that its sublattice magnetization as a function of temperature is consistent with experimental results concerned[11]. Our simulated magnetization curves shown Fig. 2 and B_c - T curves in Fig. 3 are both in good agreement with experimental curves[7]. These show that our model treatment and simulation methods are reliable and our simulated results, with parameters from experiment, are reasonable.

As for spin dynamics in SCM systems, Glauber behavior, usually with some modifications due to finite size effects, is frequently observed, and on the other hand, there are convincing evidences that quantum nucleation plays some important roles in the magnetization dynamics. Our simulated results show that both the classical thermal activation and quantum spin tunneling play important roles in determining the spin dynamics. For high temperatures, the classical thermal activation is dominating, but at very low temperatures the classical effect

becomes less important, even is frozen, so that the spin dynamics is determined mainly by the quantum spin tunneling effect.

In summary, we have made the hybrid DMC method suitable to studying the spin dynamics of SCMs with strong magnetic anisotropy, and used it to investigate temperature-dependent dynamical magnetization behaviors of the famous $[\text{Mn}_2\text{Ni}]$ SCM system. Our DMC simulated magnetization curves are in good agreement with experimental results under typical temperatures and sweeping rates. We have also calculated the coercive fields as functions of temperature and plotted B_c - T curves for typical sweeping rates. It is interesting and surprising that our simulated B_c - T curves are well consistent with experimental ones, and both of the simulated and experimental curves can be satisfactorily fitted with the simple function in Equ. (6). These means that our theory and simulated results are reasonable and reliable to other SCM systems and those made from adatoms on surfaces[1, 2, 34].

This work is supported by Nature Science Foundation of China (Grant No. 11174359), by Chinese Department of Science and Technology (Grant No. 2012CB932302), and by the Strategic Priority Research Program of the Chinese Academy of Sciences (Grant No. XDB07000000).

* Corresponding author: bgliu@iphy.ac.cn

- [1] S. Loth, S. Baumann, C. P. Lutz, D. M. Eigler, and A. J. Heinrich, *Science* **335**, 196 (2012).
- [2] E. Heintze, F. E. Hallak, C. Clauss, A. Rettori, M. G. Pini, F. Totti, M. Dressel, and L. Bogani, *Nat. Mater.* **12**, 202 (2013).
- [3] R. Clerac, H. Miyasaka, M. Yamashita, and C. Coulon, *J. Am. Chem. Soc.* **124**, 12837 (2002)
- [4] H. Miyasaka, R. Cleac, K. Mizushima, K. Sugiura, M. Yamashita, W. Wernsdorfer, and C. Coulon, *Inorg. Chem.* **42**, 8203 (2003)
- [5] W.-X. Zhang, R. Ishikawa, B. Breedlovea and M. Yamashita, *RSC Advances* **3**, 3772 (2013).
- [6] C. Coulon, R. Clerac, L. Lecren, W. Wernsdorfer, and H. Miyasaka, *Phys. Rev. B* **69**, 132408 (2004).
- [7] W. Wernsdorfer, R. Clerac, C. Coulon, L. Lecren, and H. Miyasaka, *Phys. Rev. Lett.* **95**, 237203 (2005)
- [8] J. Kishine, T. Watanabe, H. Deguchi, M. Mito, T. Sakai, T. Tajiri, M. Yamashita, and H. Miyasaka, *Phys. Rev. B* **74**, 224419 (2006)
- [9] L. Lecren, W. Wernsdorfer, Y. Li, A. Vindigni, H. Miyasaka, and R. Clerac, *J. Am. Chem. Soc.* **129**, 5045 (2007)
- [10] C. Coulon, R. Clerac, W. Wernsdorfer, T. Colin, A. Saitoh, N. Motokawa, and H. Miyasaka, *Phys. Rev. B* **76**, 214422 (2007)
- [11] C. Coulon, R. Clerac, W. Wernsdorfer, T. Colin, and H. Miyasaka, *Phys. Rev. Lett.* **102**, 167204 (2009)
- [12] O. V. Billoni, V. Pianet, D. Pescia, and A. Vindigni, *Phys. Rev. B* **84**, 064415 (2011).
- [13] M. G. Pini, A. Rettori, L. Bogani, A. Lascialfari, M. Mariani, A. Caneschi, and R. Sessoli, *Phys. Rev. B* **84**, 094444 (2011).
- [14] K. Bernot, L. Bogani, A. Caneschi, D. Gatteschi, and R. Sessoli, *J. Am. Chem. Soc.* **128**, 7948 (2006)
- [15] S. Arrhenius, *Z. Phys. Chem.* **4**, 226 (1889).
- [16] R. D. Kirby, J. X. Shen, R. J. Hardy, and D. J. Sellmyer, *Phys. Rev. B* **49**, 10810 (1994).
- [17] L. Landau, *Phys. Z. Sowjetunion* **2**, 46 (1932).
- [18] C. Zener, *Proc. R. Soc. London, Ser. A* **137**, 696 (1932).
- [19] D. Gatteschi, R. Sessoli, and J. Villain, *Molecular Nanomagnets*, Oxford University Press, New York, 2006.
- [20] D. Gatteschi and A. Vindigni, *Single-chain magnets*, in: J. Bartolome, F. Luis, and J. F. Fernandez, Ed., *Molecular Magnets - Physics and Applications*, Springer-Verlag Berlin Heidelberg 2014.
- [21] H. De Raedt, S. Miyashita, K. Saito, D. Garcia-Pablos, and N. Garcia, *Phys. Rev. B* **56**, 11761 (1997).
- [22] Q. Niu and M. G. Raizen, *Phys. Rev. Lett.* **80**, 3491 (1998).
- [23] W. Wernsdorfer, R. Sessoli, A. Caneschi, D. Gatteschi, and A. Cornia, *Europhys. Lett.* **50**, 552 (2000).
- [24] V. L. Pokrovsky and N. A. Sinitsyn, *Phys. Rev. B* **65**, 153105 (2002).
- [25] M. Jona-Lasinio, O. Morsch, M. Cristiani, N. Malossi, J. H. Muller, E. Courtade, M. Anderlini, and E. Arimondo, *Phys. Rev. Lett.* **91**, 230406 (2003).
- [26] E. Rastelli and A. Tassi, *Phys. Rev. B* **64**, 064410 (2001).
- [27] P. Földi, M. G. Benedict, J. M. Pereira, Jr., and F. M. Peeters, *Phys. Rev. B* **75**, 104430 (2007).
- [28] G.-B. Liu and B.-G. Liu, *Appl. Phys. Lett.* **95**, 183110 (2009); *Phys. Rev. B* **82**, 134410 (2010).
- [29] R. J. Glauber, *J. Math. Phys. (N.Y.)* **4**, 294 (1963).
- [30] G. Korniss, J. White, P. A. Rikvold, and M. A. Novotny, *Phys. Rev. E* **63**, 016120 (2000).
- [31] K. Park, P. A. Rikvold, G. M. Buendia, and M. A. Novotny, *Phys. Rev. Lett.* **92**, 015701 (2004).
- [32] Y. Li and B.-G. Liu, *Phys. Rev. B* **73**, 174418 (2006); *Phys. Rev. Lett.* **96**, 217201 (2006).
- [33] B.-G. Liu, K.-C. Zhang, and Y. Li, *Front. Phys. China* **2**, 424 (2007).
- [34] A. Spinelli, B. Bryant, F. Delgado, J. Fernandez-Rossier, and A. F. Otte, *Nat. Mater.* **13**, 782 (2014).